Multiplexed Electrochemical Immunoassay of Phosphorylated Proteins Based on Enzyme-Functionalized Gold Nanorod Labels and Electric Field-Driven Acceleration

ARTICLE *in* ANALYTICAL CHEMISTRY · AUGUST 2011

Impact Factor: 5.64 · DOI: 10.1021/ac2009977 · Source: PubMed

5 AUTHORS, INCLUDING:

Dan Du
Washington State University
130 PUBLICATIONS **3,747** CITATIONS
SEE PROFILE

Jun Wang
Nanjing University of Posts and Telecommu…
355 PUBLICATIONS **11,629** CITATIONS
SEE PROFILE

Donglai lu
Arizona State University
25 PUBLICATIONS **569** CITATIONS
SEE PROFILE

Yuehe Lin
Washington State University
364 PUBLICATIONS **21,422** CITATIONS
SEE PROFILE

analytical chemistry

ARTICLE

pubs.acs.org/ac

Multiplexed Electrochemical Immunoassay of Phosphorylated Proteins Based on Enzyme-Functionalized Gold Nanorod Labels and Electric Field-Driven Acceleration

Dan Du,[*,†,‡] Jun Wang,[‡] Donglai Lu,[‡] Alice Dohnalkova,[‡] and Yuehe Lin[*,‡]

[†]Key Laboratory of Pesticide and Chemical Biology of Ministry of Education, College of Chemistry, Central China Normal University, Wuhan 430079, PR China

[‡]Pacific Northwest National Laboratory, Richland, Washington 99352, United States

Supporting Information

ABSTRACT: A multiplexed electrochemical immunoassay integrating enzyme amplification and electric field-driven strategy was developed for fast and sensitive quantification of phosphorylated p53 at Ser392 (phospho-p53^{392}), Ser15 (phospho-p53^{15}), Ser46 (phospho-p53^{46}), and total p53 simultaneously. The disposable sensor array has four spatially separated working electrodes, and each of them is modified with different capture antibody, which enables simultaneous immunoassay to be conducted without cross-talk between adjacent electrodes. The enhanced sensitivity was achieved by a multienzyme amplification strategy using gold nanorods (AuNRs) as nanocarrier for coimmobilization of horseradish peroxidase (HRP) and detection antibody (Ab_2) at a high ratio of HRP/Ab_2, which produced an amplified electrocatalytic response by the reduction of HRP oxidized thionine in the presence of hydrogen peroxide. The immunoreaction processes were accelerated by applying +0.4 V for 3 min and then −0.2 V for 1.5 min; thus, the whole sandwich immunoreactions could be completed in less than 5 min. Under optimal conditions, this method could simultaneously detect phospho-p53^{392}, phospho-p53^{15}, phospho-p53^{46}, and total p53 ranging from 0.01 to 20 nM, 0.05 to 20 nM, 0.1 to 50 nM, and 0.05 to 20 nM with detection limits of 5 pM, 20 pM, 30 pM, and 10 pM, respectively. Accurate determinations of these proteins in human plasma samples were demonstrated by comparison to the standard ELISA method. The disposable immunosensor array shows excellent promise for clinical screening of phosphorylated proteins and convenient point-of-care diagnostics.

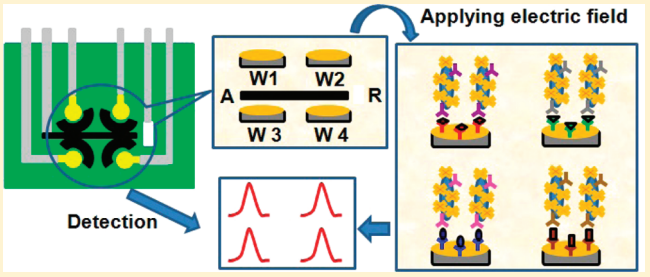

The p53 tumor suppressor protein is a potent transcription factor that plays an important role in controlling cellular responses to various stress signals such as ionizing radiation and UV induction.[1,2] Loss of p53 function results in an induction of tumors and gene mutation, which is caused by the conformational changes in p53 protein structure.[3,4] In response to stress, p53 undergoes rapid phosphorylation on several serine and threonine residues within the N- and C-terminal domains.[5] There are some results showing a clinical implication of p53 phosphorylation in human cancers.[6−10] For example, Bar's group evaluated expression of p53 protein phosphorylated at serine 20 (phospho-p53^{20}) and serine 392 (phospho-p53^{392}) involved in ovarian neoplasms.[6] Some authors reported that p53-Ser392 phosphorylation occurred preferentially in response to UV radiation, showing selective susceptibility to UV-induced skin tumors.[7,8] Yap et al. suggested that p53-Ser392 phosphorylation may regulate the oncogenic function of mutant forms of p53 protein in breast cancer.[9] A recent study reported that p53 phosphorylated on serine 15 (phospho-p53^{15}) is crucial for an ionizing radiation response and might be used as a potential biomarker of Gamma-radiation exposure since the phosphorylation is dose dependent.[10] Thus, simultaneous determination of multiple phosphorylated p53 in different phosphorylation sites is of great significance in clinical research and early diagnosis of cancers.

Multiplexed immunoassay with the advantages of shortened analysis time, simplified signals, decreased sampling volume, improved test efficiency, and reduced cost as compared to parallel single-analyte assays is a promising analytical method in protein analysis.[11−13] Electrochemical immunosensor assay (EIA) has gained considerable interest as a bioanalytical method in recent years because of the advantages of simple instrumentation, easy signal quantification, low cost of the entire assay, and convenient miniaturization. Various EIA formats have been devised to realize simultaneously multiplexed analysis, using either multiple labels or spatial resolution to discriminate between the different analytes.[14,15] Multiple labels, one for each analyte, use different enzymes,[16] metal ions,[17] and nanoparticles.[18] An alternate strategy for EIA can be performed by

Received: April 18, 2011
Accepted: July 28, 2011
Published: July 28, 2011

use of a single-enzyme label,[11,13,15] which offers an advantage in simplicity as compared to multiple labels but requires sufficient separation to prevent signal interference (cross-talk) between neighboring electrodes. Wilson has described enough spatial separation of electrodes which can perform individual immunoassay of multiple proteins without amperometric cross-talk.[11,15,19] Ju's group immobilized an electron-transfer mediator on the electrode to avoid cross-talk when a single-enzyme label for multiplexed immunoassay of proteins was used.[14,20]

Various signal amplification technologies using nanomaterials have been developed for ultrasensitive detection of proteins.[21−23] One of the most popular strategies is enzyme-functionalized nanoparticles used as tracers to enhance the sensitivity of detection by loading a large amount of enzymes toward an individual sandwich immunological reaction event. These nanomaterials include carbon nanotubes (CNTs),[24,25] carbon nanospheres,[26] graphene oxide,[27] gold nanoparticles (GNPs),[13] silica nanoparticles,[28] and carboxylated magnetic beads.[29] For example, Rusling's group[24,25] has achieved greatly enhanced sensitivity using bioconjugates featuring horseradish peroxidase (HRP) labels and signal antibodies linked to CNTs for immunodetection of the prostate specific antigen and interleukin-6, respectively. Our group has developed a sensitive immunosensor for α-fetoprotein based on carbon nanosphere/HRP labeling.[26]

A fast immunoassay is highly desired for detection of proteins. In order to accelerate the immunoreactions on an immunosensor, many technologies such as magnetic stirring,[30] low-power microwave radiation,[31] and electric field-driven[32] and electrophoresis-assisted immunoassay[33,34] have been explored. Among these technologies, the electric field-driven method, which has been used to control nucleic acid hybridization, is an excellent enrichment and acceleration strategy for the transport of low-abundant protein.

Here, we report a multiplexed EIA by combining an enzyme-label amplification strategy with an electric field-driven acceleration method for simultaneous detection of multiple phosphorylated proteins. Gold nanorods (AuNRs) have strong surface plasmon absorption which led to interest in their use in biodiagnostics or for selective targeting in photothermal thearapeutics.[35] Here, we demonstrate AuNRs as nanocarrier to allow coimmobilization of HRP and detection antibody (Ab_2) to form HRP/Ab_2-AuNRs bioconjugates. Positive driving potential was applied to accelerate the transport of negatively charged antigens ($p53^{392}$, $p53^{15}$, $p53^{46}$, and p53) to the electrode surface, and then, a low negative driving potential was applied to accelerate the transport of positively charged HRP/$p53^{392}Ab_2$-AuNRs, HRP/$p53^{15}Ab_2$-AuNRs, HRP/$p53^{46}Ab_2$-AuNRs, and HRP/p53Ab_2-AuNRs bioconjugates to form sandwich immunocomplexes on each working electrode, respectively. Greatly amplified sensitivity and shortened time are achieved by enzyme amplification and electric forces. Cross-talk is eliminated by spatial separation between adjacent electrode and antibody locations. This easily fabricated biochip shows great promise for rapid and sensitive detection of other proteins and clinical applications.

EXPERIMENTAL METHODS

Reagents and Materials. Human phospho-p53 (S392) ELISA kit, Human phospho-p53 (S15) ELISA kit, Human phospho-p53 (S46) ELISA kit, and Human total p53 ELISA kit were purchased from R&D Systems Inc. Gold nanorods (AuNRs, 35 μg mL^{-1}), bovine serum albumin (BSA), Triton X-100, Tween-20, thionine, 3,3′,5,5′-tetramethylbenzidine (TMB), and phosphate buffer saline (PBS) were acquired from Sigma/Aldrich. *N*-Hydroxysuccinimide-activated hexa(ethylene glycol) undecane Thiol (NHS) was obtained from NanoScience Instrument Inc.

Scheme 1. Schematic Illustration of Multiplexed Electrochemical Immunoassay by an Electric Field-Driven Process and Multienzymes Labeling Amplification Strategy Using HRP-Ab_2-AuNRs Conjugates

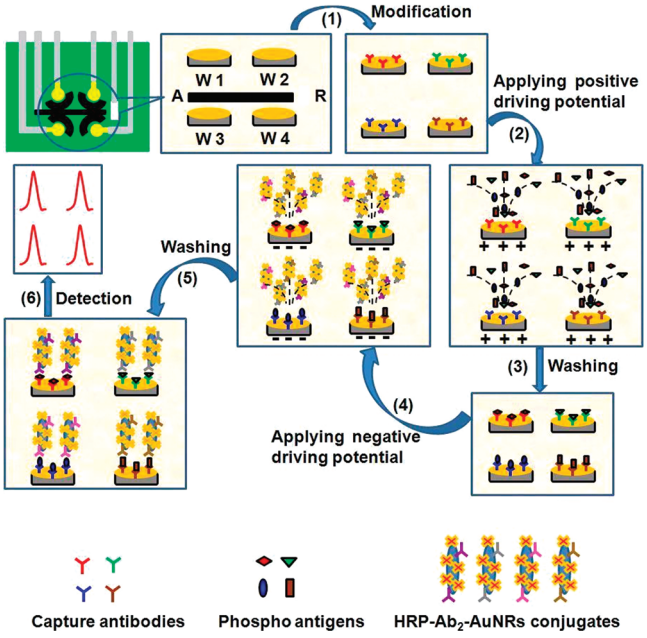

Apparatus. Electrochemical experiments, including cyclic voltammetry (CV) and square wave voltammetry (SWV), were performed with an electrochemical analyzer CHI 660A (CH Instruments, Austin, TX) connected to a personal computer. UV−vis measurements were carried out on a Safire 2 microplate reader (TECAN, Switzerland). Transmission electron microscopy (TEM) images were carried out on a Jeol JEM 2010 microscope at 200 keV. All images were digitally recorded with a slow-scan charged coupled devices camera (image size 1024 × 1024 pixels).

Preparation of HRP-Ab_2-AuNRs Bioconjugates. The concentrations of active HRP in the stock HRP-$p53^{392}Ab_2$-AuNRs, HRP-$p53^{15}Ab_2$-AuNRs, HRP-$p53^{46}Ab_2$-AuNRs, and HRP-p53Ab_2-AuNRs dispersion were determined as 4.52 μg mL^{-1}, 4.27 μg mL^{-1}, 4.03 μg mL^{-1}, and 4.73 μg mL^{-1}, respectively. (See Supporting Information.)

Fabrication of Immunosensor Array. See Supporting Information.

Simultaneous Immunoassay Procedure. A sandwich immunoassay was used for simultaneous determination of four proteins (phospho-$p53^{392}$, phospho-$p53^{15}$, phospho-$p53^{46}$, and p53). (See Supporting Information.)

RESULTS AND DISCUSSION

Fast Enrichment and Signal Amplification Concept for Multiplexed Immunoassay. As shown in Scheme 1, the sandwich

dx.doi.org/10.1021/ac2009977 |*Anal. Chem.* 2011, 83, 6580–6585

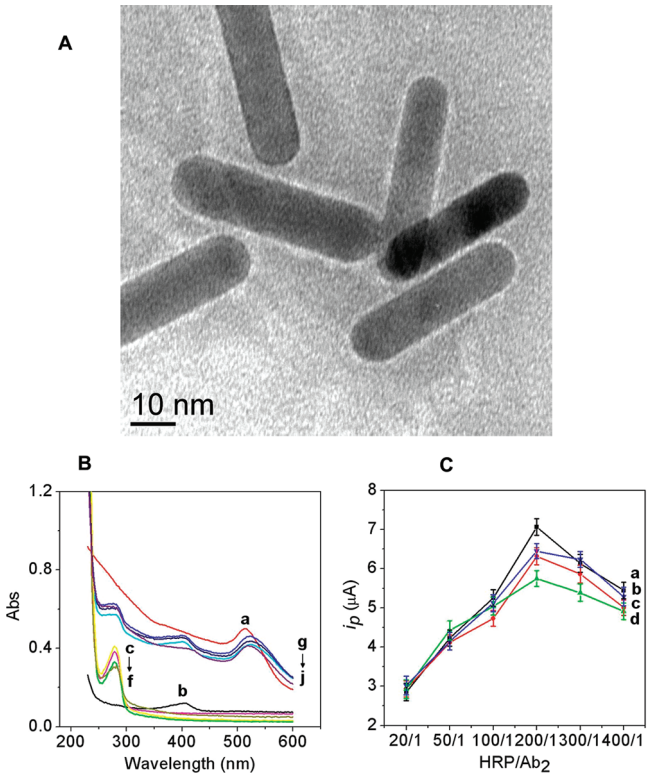

Figure 1. (A) TEM image of the HRP-p53^{392}Ab$_2$-AuNRs conjugate. (B) UV−vis spectra of (a) AuNRs, (b) HRP, (c) p53^{392}Ab$_2$, (d) p53^{15}Ab$_2$, (e) p53^{46}Ab$_2$, and (f) p53Ab$_2$ and (g) HRP-p53^{392}Ab$_2$-AuNRs, (h) HRP-p53^{15}Ab$_2$-AuNRs, (i) HRP-p53^{46}Ab$_2$-AuNRs, and (j) HRP-p53Ab$_2$-AuNRs conjugates. (C) Effects of (a) HRP/p53^{392}Ab$_2$, (b) HRP/p53^{15}Ab$_2$, (c) HRP/p53^{46}Ab$_2$, and (d) HRP/p53Ab$_2$ ratio on the response currents. 1.0 ng mL^{-1} phospho-p53^{392}, phospho-p53^{15}, phospho-p53^{46}, and p53 antigen solutions were used during the incubation process.

immunoreaction was driven by applying positive and negative potentials, respectively. Because the isoelectric points (PIs) of phospho-p53^{392}, phospho-p53^{15}, phospho-p53^{46}, and p53 are around 5, all the antigens will be negatively charged in pH 7.0 PBS. When a positive driving potential was applied, an electric field would be generated near the surface of the immunosensor. The second immunoreaction was driven by applying a negative potential to accelerate the transport of HRP-p53^{392}Ab$_2$-AuNRs, HRP-p53^{15}Ab$_2$-AuNRs, HRP-p53^{46}Ab$_2$-AuNRs, and HRP-p53Ab$_2$-AuNRs bioconjugates to the electrode surface. Since the PI of HRP is 8−9, the high ratio of HRP/Ab$_2$ on the AuNRs makes the net charge of HRP-Ab$_2$-AuNRs conjugates positive in pH 7.0 PBS and can be accelerated by negative electric force. With this two-step electric field driving, the immunoreaction time was greatly shortened, leading to a very rapid immunodetection. The residual and nonspecific adsorption was removed by washing with 0.05% Tween-20 and PBS buffer.

To enhance the detection sensitivity, we pursued a multi-enzymes labeling strategy instead of a singly enzyme label during immunoassay. Here, AuNRs served as nanocarriers allowing coimmobilization of Ab$_2$ and a large amount of HRP. Greatly amplified response was achieved using HRP/Ab$_2$-AuNRs bioconjugates instead of conventional HRP/Ab$_2$ conjugate in ELISA.

Characterization of HRP/Ab$_2$-AuNRs Bioconjugates. To confirm the attachment of proteins onto AuNRs, negatively stained sample was prepared for TEM to study the size and distribution of HRP/Ab$_2$-AuNRs bioconjugates. As can be seen from Figure 1, individual nanorods were clearly identifiable with a diameter about 10 nm and a length about 50 nm (panel A). They were obviously surrounded by a layer of protein (white), indicating successful coimmobilization of Ab$_2$ and HRP onto the AuNRs surface.

The resulting HRP-p53^{392}Ab$_2$-AuNRs, HRP-p53^{15}Ab$_2$-AuNRs, HRP-p53^{46}Ab$_2$-AuNRs, and HRP-p53Ab$_2$-AuNRs bioconjugates were further characterized by UV−vis spectroscopy. As shown in Figure 1B, an obvious absorption peak at 510 nm (curve a) was observed, which is the typical resonance band of AuNRs. Pure HRP, p53^{392}Ab$_2$, p53^{15}Ab$_2$, p53^{46}Ab$_2$, and p53Ab$_2$ displayed absorption peaks at 404 nm (curve b) and 280 nm (curves c, d, e, f), respectively. When p53^{392}Ab$_2$, p53^{15}Ab$_2$, p53^{46}Ab$_2$, and p53Ab$_2$ together with HRP were bound to AuNRs, three obvious absorption peaks were observed on the resulting HRP-p53^{392}Ab$_2$-AuNRs (curve g), HRP-p53^{15}Ab$_2$-AuNRs (curve h), HRP-p53^{46}Ab$_2$-AuNRs (curve i), and HRP-p53Ab$_2$-AuNRs (curve j), indicating successful binding of Ab$_2$ and HRP onto AuNRs.

The ratio of HRP and Ab$_2$ (HRP/Ab$_2$) is the most important factor on the response signal. As shown in Figure 1C, one can see that all electrocatalytic currents on four electrodes increased with increasing HRP/Ab$_2$, and the maximum responses were achieved at the ratio of 200/1. Although the increased amount of HRP can enhance the current response, it will decrease the amount of Ab$_2$ on AuNRs surface due to the limited loading capacity and, therefore, decrease the immuno-efficiency resulting in a decreased response. Thus, 200/1 of the HRP/Ab$_2$ was used to prepare the HRP-Ab$_2$-AuNRs conjugate.

Fast Multiplexed Electrochemical Immunoassay. Multiplexed EIA was achieved by performing each electrode as an independent immunosensor for a specific antigen. Here, p53^{392}, p53^{15}, p53^{46}, and p53 capture antibody (p53^{392}Ab$_1$, p53^{15}Ab$_1$, p53^{46}Ab$_1$, p53Ab$_1$) were first attached onto each working electrode through a layer of NHS, respectively. As shown in Figure 2, the cyclic voltammograms at screen printed gold electrodes array (SPGEA) (curves a$_{(1-4)}$ in CH1-CH4) did not show any detectable signal, while the background currents increased after the formation of p53^{392}Ab$_1$/NHS/SPGEA, p53^{15}Ab$_1$/NHS/SPGEA, p53^{46}Ab$_1$/NHS/SPGEA, and p53-Ab$_1$/NHS/SPGEA (curves b$_{(1-4)}$ in CH1-CH4) due to the change of surface charge and relatively rough surface. Upon adding 25 μM thionine and 2 mM H_2O_2 to the PBS buffer, the cyclic voltammogram at four modified working electrodes exhibited a pair of stable and well-defined redox peaks at −0.238 V and −0.256 V (curves c$_{(1-4)}$ in CH1-CH2), respectively, in four channels which correspond to the electrochemical oxidation and reduction of thionine. With the two-step electric field driving during the sandwich immuno-recognition processes, the resulting HRP-p53^{392}Ab$_2$-AuNRs/phospho-p53^{392}/p53^{392}Ab$_1$/NHS/SPGEA, HRP-p53^{15}Ab$_2$-AuNRs/phospho-p53^{15}/p53^{15}-Ab$_1$/NHS/SPGEA, HRP-p53^{46}Ab$_2$-AuNRs/phospho-p53^{46}/p53^{46}Ab$_1$/NHS/SPGEA, and HRP-p53Ab$_2$-AuNRs/p53/p53-Ab$_1$/NHS/SPGEA displayed an obvious increase in electrocatalytic reduction current (curves d$_{(1-4)}$ in CH1-CH2). It is not surprising that the enhanced signal was ascribed to the introduction of a large amount of enzymes onto the electrode surface using AuNRs as nanocarriers. This amplified electrocatalytic responses come from the reduction of the oxidized thionine(ox), which is produced by HRP in the presence of hydrogen peroxide.

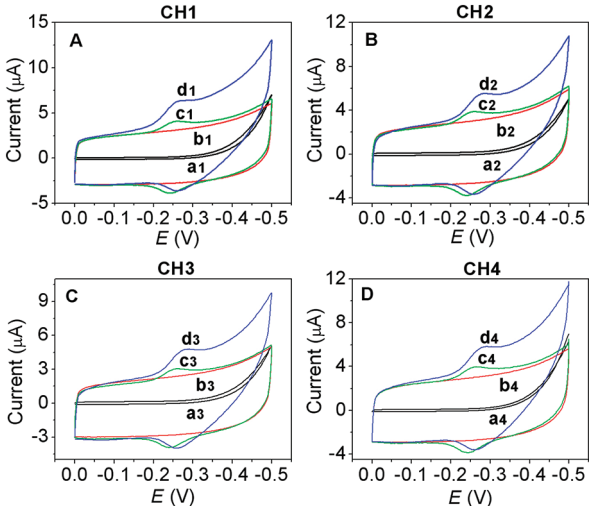

Figure 2. Cyclic voltammograms obtained at (A) CH1 for phospho-p53^{392} target, (B) CH2 for phospho-p53^{15} target, (C) CH3 for phospho-p53^{46} target, and (D) CH4 for p53 target. (a_1−a_4): SPGEA on four channels in pH 7.0 PBS; (b_1−b_4): p53^{392}Ab$_1$/NHS/SPGEA, p53^{15}Ab$_1$/NHS/SPGEA, p53^{46}Ab$_1$/NHS/SPGEA, and p53Ab$_1$/NHS/SPGEA in pH 7.0 PBS; (c_1−c_4): (b_1−b_4) in pH 7.0 PBS containing 25 μM thionine and 2 mM H_2O_2; (d_1−d_4): HRP-p53^{392}Ab$_2$-AuNRs/phospho-p53^{392}/p53^{392}Ab$_1$/NHS/SPGEA, HRP-p53^{15}Ab$_2$-AuNRs/phospho-p53^{15}/p53^{15}Ab$_1$/NHS/SPGEA, HRP-p53^{46}Ab$_2$-AuNRs/phospho-p53^{46}/p53^{46}Ab$_1$/NHS/SPGEA, and HRP-p53Ab$_2$-AuNRs/p53/p53Ab$_1$/NHS/SPGEA in pH 7.0 PBS containing 25 μM thionine and 2 mM H_2O_2.

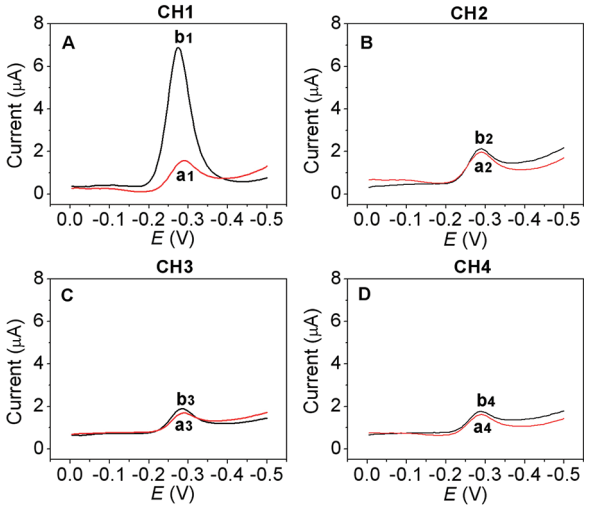

Figure 3. Cyclic voltammograms obtained at (A) CH1 for phospho-p53^{392} target, (B) CH2 for phospho-p53^{15} target, (C) CH3 for phospho-p53^{46} target, and (D) CH4 for p53 target. (a_1−a_4): p53^{392}Ab$_1$/NHS/SPGEA, p53^{15}Ab$_1$/NHS/SPGEA, p53^{46}Ab$_1$/NHS/SPGEA, and p53Ab$_1$/NHS/SPGEA in pH 7.0 PBS containing 25 μM thionine and 2 mM H_2O_2; (b_1−b_4): HRP-p53^{392}Ab$_2$-AuNRs/phospho-p53^{392}/p53^{392}Ab$_1$/NHS/SPGEA in pH 7.0 PBS containing 25 μM thionine and 2 mM H_2O_2 after incubating with only 1.0 ng mL^{-1} phospho-p53^{392} antigen solution and all HRP-p53^{392}Ab$_2$-AuNRs, HRP-p53^{15}Ab$_2$-AuNRs, HRP-p53^{46}Ab$_2$-AuNRs, and HRP-p53Ab$_2$-AuNRs conjugates.

Since thionine(ox) is only generated near an electrode, it is likely that most of the thionine(ox) will be electrochemically reduced as soon as it is formed and will not diffuse from the electrode.

Evaluation of Cross-Talk between Electrodes. The simultaneous multianalyte immunoassay uses arrays of immunosensing electrodes, each capable of measuring a specific analyte using an electrochemical substrate. In this assay, thionine(ox) generated by HRP and H_2O_2 is electrochemically reduced by the sensing electrodes and produces a quantitative amperometric current that is proportional to the target analyte concentration. Thionine(ox) is generated only at electrodes that contain bound HRP and, therefore, only at electrodes that contain bound target antigens. The assays rely on the spatial separation between different electrode and antibody locations to establish simultaneous measurements without cross-talk between electrodes. We can also estimate the possible cross-talk according to the diffusion of thionine(ox) between adjacent electrodes. It is known that the diffusion coefficient of thionine is 2.2×10^{-6} cm^2 s^{-1}.[36] According to Einstein's diffusion equation ($d = (2Dt)^{1/2}$) in which d is average distance traveled (cm), D is diffusion coefficient, and t is time (s), it can predict that thionine will diffuse less than 0.6 mm in 10 min. Since the adjacent working electrodes are separated by a distance of 3 mm and the measuring time is ~2 min, cross-talk between electrodes will be negligible. In addition, since thionine(ox) is only produced in proximity to the electrode surface and so is efficiently captured by the electrode, it is likely that most of the thionine(ox) will be electrochemically reduced as soon as it is formed and will not diffuse from the electrode.

To confirm that electrochemical cross-talk was not occurring between neighboring electrodes, the immunosensor was incubated in a series of solutions containing only one protein marker and the amperometric responses in four channels were recorded simultaneously. As shown in Figure 3, only the immunosensor for the corresponding antigen (phospho-p53^{392}) in the incubation solution showed a significant increase in reduction current (panel A) while the others produced almost the same signal as normal background response (panels B, C, D). The measurement was also taken in other antigen solutions, and only the corresponding working electrode produced an increase in the reduction current while no changed signals were observed on other working electrodes (data not shown). Even no obvious increase in current response can be observed on the neighboring electrode for 20 min following the addition of thionine and H_2O_2. The result proved that cross-talk at the array was negligible, and multiplexed immunoassay in a single run was possible without influence by adjacent electrodes.

Optimization for Electric Field-Driven Incubation. The immunoreaction rates are highly related to the transport rates of the corresponding antigens and HRP-Ab$_2$-AuNRs conjugates to the immunosensor surface. The driving potential and driving time were optimized as +0.4 V for 3 min and −0.2 V for 1.5 min. (See Supporting Information, Figure S1.)

Simultaneous Immunoassay of Proteins. Under the optimized conditions, the proposed immunosensor array was evaluated with different concentrations of phospho-p53^{392}, phospho-p53^{15}, phospho-p53^{46}, and total p53 in the incubation mixture. As shown in Figure 4, the SWV peaks in four channels increased with the increase of antigen concentrations, respectively (A−D). The linear responses were obtained over the phospho-p53^{392} concentration range from 0.01 to 20 nM with the detection limit of 5 pM (E), phospho-p53^{15} concentrations range from 0.05 to 20 nM with the detection limit of 20 pM (F),

dx.doi.org/10.1021/ac2009977 |Anal. Chem. 2011, 83, 6580–6585

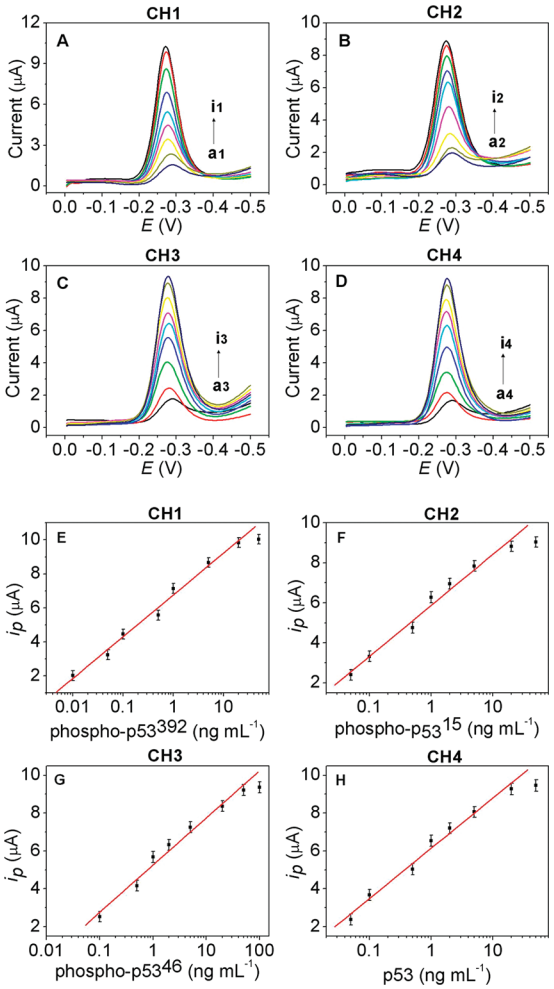

Figure 4. SWV curves in pH 7.0 PBS containing 25 μM thionine and 2 mM H_2O_2. (A) HRP-p53^{392}Ab$_2$-AuNRs/phospho-p53^{392}/p53^{392}Ab$_1$/NHS/SPGEA after incubation with (a_1) 0, (b_1) 0.01, (c_1) 0.05, (d_1) 0.1, (e_1) 0.5, (f_1) 1.0, (g_1) 5.0, (h_1) 20, and (i_1) 50 ng mL^{-1} phospho-p53^{392} antigen; (B) HRP-p53^{15}Ab$_2$-AuNRs/phospho-p53^{15}/p53^{15}Ab$_1$/NHS/SPGEA after incubation with (a_2) 0, (b_2) 0.05, (c_2) 0.1, (d_2) 0.5, (e_2) 1.0, (f_2) 2.0, (g_2) 5.0, (h_2) 20, and (i_2) 50 ng mL^{-1} phospho-p53^{392} antigen; (C) HRP-p53^{46}Ab$_2$-AuNRs/phospho-p53^{46}/p53^{46}Ab$_1$/NHS/SPGEA after incubation with (a_3) 0, (b_3) 0.1, (c_3) 0.5, (d_3) 1.0, (e_3) 2.0, (f_3) 5.0, (g_3) 20, (h_3) 50, and (i_3) 100 ng mL^{-1} phospho-p53^{392} antigen; (D) HRP-p53Ab$_2$-AuNRs/p53/p53Ab$_1$/NHS/SPGEA after incubation with (a_4) 0, (b_4) 0.05, (c_4) 0.1, (d_4) 0.5, (e_4) 1.0, (f_4) 2.0, (g_4) 5.0, (h_4) 20, and (i_4) 50 ng mL^{-1} p53 antigen. Calibration curves of the immunosensor array for detection of (E) phospho-p53^{392} antigen; (F) phospho-p53^{15} antigen; (G) phospho-p53^{46} antigen, and (H) p53 antigen.

phospho-p53^{46} concentrations range from 0.1 to 50 nM with the detection limit of 30 pM (G), and p53 concentrations range from 0.05 to 20 nM with the detection limit of 10 pM (H). The linear calibration curves were $i_p(\mu A)$ = 2.61 + 6.93 lgc (phospho-p53^{392}, ng/mL), $i_p(\mu A)$ = 5.88 + 2.55 lgc (phospho-p53^{15}, ng/mL), $i_p(\mu A)$ = 5.25 + 2.49 lgc (phospho-p53^{46}, ng/mL), and $i_p(\mu A)$ = 6.14 + 2.66 lgc (p53, ng/mL), respectively. Comparably, we used the ELISA method for detecting phospho-p53^{392}, phospho-p53^{15}, phospho-p53^{46}, and total p53, and the results were listed in Table 1. It reveals that the proposed multienzyme labeling amplification strategy possesses the advantages of both higher sensitivity and wider linear range than that of ELISA. The detection limit of this immunosensor was even 2-fold lower than our previous result using graphene oxide as nanocarrier.[27]

Table 1. Comparison of Proposed Immunosensor and ELISA Methods

	immunosensor array		ELISA	
	linear range	detection limit	linear range	detection limit
phospho-p53^{392}	0.01−20 ng/mL	5 pg/mL	0.05−3 ng/mL	20 pg/mL
phospho-p53^{15}	0.05−20 ng/mL	20 pg/mL	0.3−20 ng/mL	60 pg/mL
phospho-p53^{46}	0.1−50 ng/mL	30 pg/mL	0.6−20 ng/mL	100 pg/mL
p53	0.05−20 ng/mL	10 pg/mL	0.1−8.0 ng/mL	40 pg/mL

Reproducibility and Stability of the Immunosensor Array. The reproducibility of the proposed immunosensor array was evaluated by intra- and interassay coefficients of variation (CVs). The intra-assay precision of the analytical method was examined by analyzing one immunosensor array for six replicate determinations. The CVs of the intra-assay were 4.1%, 3.6%, 5.7%, and 5.4% at 1.0 ng mL^{-1} phospho-p53^{392}, phospho-p53^{15}, phospho-p53^{46}, and p53, respectively. The interassay CVs on six immunosensors were 7.3%, 6.8%, 6.5%, and 6.9% at 1.0 ng mL^{-1} phospho-p53^{392}, phospho-p53^{15}, phospho-p53^{46}, and p53, respectively. These results demonstrated acceptable reproducibility and precision of the proposed immunosensor array.

The immunosensor array could be stored at 4 °C. In this way, no detectable loss of the initial response was observed for 3 days; over 90% of the initial response remained after one week, and 85% remained after one month, indicating acceptable stability.

CONCLUSIONS

In this paper, an immunosensor array integrating enzymatic amplification with electric field-driven strategy for fast and sensitive multiplexed immunodetection of proteins was developed. The simultaneous immunoassay was achieved by: (1) spatial separation of the working electrode, which allowed individual immunoassays to be performed at each electrode without cross-talk interference; (2) the use of AuNRs as nanocarriers to link enzyme and detection antibody at high ratio, which produced an amplified electrocatalytic response; (3) the application of electric forces to accelerate the transport of proteins to the electrode surface, which greatly shortened the incubation time, leading to a very rapid immunodetection; (4) the reversed electric field applied during the second step repelled the weak nonspecific adsorption, leading to a better selectivity. The proposed immunosensor array shows excellent performance for simultaneous detection of proteins with wide linear ranges and low detection limit and acceptable stability, reproducibility, and accuracy. This method can be extended for determination of other proteins and meet the requirements of clinical diagnostics with simplicity, low cost, and rapidness.

ASSOCIATED CONTENT

Supporting Information. Additional information as noted in text. This material is available free of charge via the Internet at http://pubs.acs.org.

AUTHOR INFORMATION

Corresponding Authors
*E-mail: dudan@mail.ccnu.edu.cn (D.D.); yuehe.lin@pnl.gov (Y.L.).

ACKNOWLEDGMENT

This work was supported partially by Grant U54 ES16015 from the National Institute of Environmental Health Sciences, the National Institute of Health (NIH), and Grant U01 NS058161-01 from the NIH CounterACT Program through the National Institute of Neurological Disorders and Stroke. Its contents are solely the responsibility of the authors and do not necessarily represent the official views of the federal government. D.D. acknowledges the support from National Natural Science Foundation of China (21075047), the Program for Chenguang Young Scientist for Wuhan (200950431184), and the Special Fund for Basic Scientific Research of Central Colleges (CCNU10A02005). PNNL is operated for the U.S. Department of Energy (DOE) by Battelle under Contract DE-AC05-76RL01830. The materials characterization was performed at the Environmental Molecular Sciences Laboratory, a national scientific user facility sponsored by DOE's office of Biological and Environmental Research located at PNNL.

REFERENCES

(1) Vousden, K. H.; Lane, D. P. *Nat. Rev. Mol. Cell. Biol.* **2007**, *8*, 275–283.
(2) Toledo, F; Wahl, G. M. *Nat. Rev. Cancer* **2006**, *6*, 909–923.
(3) Appella, E.; Anderson, C. W. *Eur. J. Biochem.* **2001**, *268*, 2764–2772.
(4) Bode, A. M.; Dong, Z. *Nat. Rev. Cancer* **2004**, *4*, 793–805.
(5) Minamoto, T.; Buschmann, T.; Habelhah, H.; Matusevich, E.; Tahara, H.; Boerresen-Dale, A. L.; Harris, C.; Sidransky, D.; Ronai, Z. *Oncogene* **2001**, *20*, 3341–3347.
(6) Bar, J. K.; Słomska, I.; Rabczyński, J.; Noga, L.; Gryboś, M. *Int. J Gynecol. Cancer* **2009**, *19*, 1322–1328.
(7) Kapoor, M.; Lozano, G. *Proc. Natl. Acad. Sci. U.S.A.* **1998**, *95*, 2834–2837.
(8) Lu, H.; Taya, Y.; Ikeda, M.; Levine, A. J. *Proc. Natl. Acad. Sci. U.S.A.* **1998**, *95*, 6399–6402.
(9) Yap, D. B. S.; Hsieh, J. K.; Zhong, S.; Heath, V.; Gusterson, B.; Crook, T.; Lu, X. *Cancer Res.* **2004**, *64*, 4749–4754.
(10) Tichy, A.; Zaškodova, D.; Zoelzer, F.; Vavrova, J.; Šinkorova, Z.; Pejchal, J.; Osterreicher, J.; Řezačova, M. *Folia Biol.* **2009**, *55*, 41–44.
(11) Wilson, M. S. *Anal. Chem.* **2005**, *77*, 1496–1502.
(12) Tang, D. P.; Yuan, R.; Chai, Y. Q. *Clin. Chem.* **2007**, *53*, 1323–1329.
(13) Lai, G. S.; Yan, F.; Ju, H. X. *Anal. Chem.* **2009**, *81*, 9730–9736.
(14) Fu, Z. F.; Liu, H.; Ju, H. X. *Anal. Chem.* **2006**, *78*, 6999–7005.
(15) Wilson, M. S.; Nie, W. *Anal. Chem.* **2006**, *78*, 6476–6483.
(16) Kricka, L. J. *Clin. Chem.* **1992**, *38*, 327–328.
(17) Hayes, F. J.; Halsall, H. B.; Heineman, W. R. *Anal. Chem.* **1994**, *66*, 1860–1865.
(18) Liu, G.; Wang, J.; Kim, J.; Jan, M. R. *Anal. Chem.* **2004**, *76*, 7126–7130.
(19) Wilson, M. S.; Nie, W. *Anal. Chem.* **2006**, *78*, 2507–2513.
(20) Wu, J.; Yan, F.; Tang, J. H.; Zhai, C.; Ju, H. X. *Clin. Chem.* **2007**, *53*, 1495–1502.
(21) (a) Wang, J.; Liu, G. D.; Engelhard, M. H.; Lin, Y. H. *Anal. Chem.* **2006**, *78*, 6974–6979. (b) Liu, G.; Wu, H.; Wang, J.; Lin, Y. H. *Small* **2006**, *2*, 1139–1143.
(22) Wang, J.; Liu, G. D.; Lin, Y. H. *Small* **2006**, *2*, 1134–1138.
(23) (a) Cui, R. J.; Liu, C.; Shen, J. M.; Gao, D.; Zhu, J. J.; Chen, H. Y. *Adv. Funct. Mater.* **2008**, *18*, 2197–2204. (b) Wang, J.; Liu, G.; Wu, H.; Lin, Y. H. *Small* **2008**, *4*, 82–86.
(24) Yu, X.; Munge, B.; Patel, V.; Jensen, G.; Bhirde, A.; Gong, J. D.; Kim, S. N.; Gillespie, J.; Gutkind, J. S.; Papadimitrakopoulos, F.; Rusling, J. F. *J. Am. Chem. Soc.* **2006**, *128*, 11199–11205.
(25) Malhotra, R.; Patel, V.; Vaque, J. P.; Gutkind, J. S.; Rusling, J. F. *Anal. Chem.* **2010**, *82*, 3118–3123.
(26) Du, D.; Zou, Z. X.; Shin, Y.; Wang, J.; Wu, H.; Engelhard, M. H.; Liu, J.; Aksay, I. A.; Lin, Y. H. *Anal. Chem.* **2010**, *82*, 2989–2995.
(27) Du, D.; Wang, L. M.; Shao, Y. Y.; Wang, J.; Engelhard, M. H.; Lin, Y. H. *Anal. Chem.* **2011**, *83*, 746–752.
(28) Wu, Y. F.; Chen, C. L.; Liu, S. Q. *Anal. Chem.* **2009**, *81*, 1600–1607.
(29) Mani, V.; Chikkaveeraiah, B. V.; Patel, V.; Gutkind, J. S.; Rusling, J. F. *ACS Nano* **2009**, *3*, 585–594.
(30) Tanaka, K.; Imagawa, H. *Talanta* **2005**, *68*, 437–441.
(31) Previte, M. J. R.; Aslan, K.; Malyn, S. N.; Geddes, C. D. *Anal. Chem.* **2006**, *78*, 8020–8027.
(32) Wu, J.; Yan, Y. T.; Yan, F.; Ju, H. X. *Anal. Chem.* **2008**, *80*, 6072–6077.
(33) Morozov, V. N.; Morozova, T. Y. *Anal. Chem.* **2003**, *75*, 6813–6819.
(34) Morozov, V. N.; Morozova, T. Y. *Anal. Chim. Acta* **2006**, *564*, 40–52.
(35) Pissuwan, D.; Valenzuela, S.; Cortie, M. B. *Biotechnol. Genet. Eng. Rev.* **2008**, *25*, 93–112.
(36) Kaneko, M. New Solid Medium for Electrochemistry and Its Application to Dye-Sensitized Solar Cells. In *Trends in Electrochemistry Research*; Nunez, M., Ed.; Nova Science Publishers, Inc.: New York, 2007; Chapter 2, pp 77.